Pergamon

Geochimica et Cosmochimica Acta, Vol. 68, No. 7, pp. 1661–1675, 2004

0016-7037/04 $30.00 + .00

doi:10.1016/j.gca.2003.09.009

The formation of chondrules by open-system melting of nebular condensates

BOSMAT A. COHEN,[1,*] ROGER H. HEWINS,[1] and CONEL M. O'D. ALEXANDER[2]

[1]Dept. of Geological Sciences, Rutgers University, 610 Taylor Rd., Piscataway, NJ 08855, USA
[2]Dept. of Terrestrial Magnetism, Carnegie Institution of Washington, 5241 Broad Branch Rd. N.W., Washington DC 20015, USA

(*Received January* 30, 2003; *accepted in revised form September* 17, 2003)

Abstract—Experiments were conducted under canonical nebular conditions to see whether the chemical compositions of the various chondrule types can be derived from a single CI-like starting material by open-system melting and evaporation. Experimental charges, produced at 1580 °C and P_{H2} of 1.31×10^{-5} atm over 1 to 18 hours, consisted of only two phases, porphyritic olivine crystals in glass. Sulfur, metallic-iron and alkalis were completely evaporated in the first minutes of the experiments and subsequently the main evaporating liquid oxides were FeO and SiO_2. Olivines from short runs (2–4 hours) have compositions of Fo_{83}-Fo_{89}, as in Type IIA chondrules, while longer experimental runs (12–18 hours) produce ~Fo_{99} olivine, similar to Type IA chondrules. The concentration of CaO in both olivine (up to 0.6 wt.%) and glass, and their Mg#, increased with increasing heating duration. Natural chondrules also show increasing CaO with decreasing S, alkalis, FeO and SiO_2. The similarities in bulk chemistry, mineralogy and textures between Type IIA and IA chondrules and the experimental charges demonstrate that these chondrules could have formed by the evaporation of CI precursors. The formation of silica-rich chondrules (IIB and IB) by evaporation requires a more pyroxene-rich precursor.

Based on the FeO evaporation rates measured here, Type IIA and IA chondrules, were heated for at least ~0.5 and ~3.5 h, respectively, if formed at 1580 °C and P_{H2} of 1.31×10^{-5} atm. Type II chondrules may have experienced higher cooling-rates and less evaporation than Type I.

The experimental charges experienced free evaporation and exhibited heavy isotopic enrichments in silicon, as well as zero concentrations of S, Na and K, which are not observed in natural chondrules. However, experiments on potassium-rich melts at the same pressure but in closed capsules showed less evaporation of K, and less K isotopic mass fractionation, than expected as a function of decreasing cooling rate. Thus the environment in which chondrules formed is as important as the kinetic processes they experienced. If chondrule formation occurred under conditions in which evaporated gases remained in the vicinity of the residual melts, the extent of evaporation would be reduced and back reaction between the gas and the melt could contribute to the suppression of isotopic mass fractionation. Hence chondrule formation could have involved evaporative loss without Rayleigh fractionation. Volatile-rich Type II and volatile-poor Type I chondrules may have formed in domains with high and low chondrule concentrations, and high partial pressures of lithophile elements, respectively.

1. INTRODUCTION

Chondrules are the main constituent in many chondrites, and are composed of silicate, metal and sulfide minerals and glass. Their textures indicate crystallization from a completely or near-completely melted state. The chemical and isotopic compositions and textures of chondrules (e.g., Brearley and Jones, 1998) are therefore a record of high temperature event(s) in the early solar system. Chondrule chemical compositions vary widely between iron-poor and iron-rich chondrules (Type I and Type II, respectively), as well as between silica-poor and silica-rich chondrules (suffix A and B respectively) (McSween, 1977a). According to the "standard model," chondrules formed by the melting of solar nebular condensates that accreted into dusty clumps, rather than by planetary melting mechanisms or by direct condensation of liquids (Grossman, 1988). Some controversy persists regarding the process responsible for the heating (Boss, 1996), the possibility of liquid condensation (Ebel and Grossman, 1997, 2000; Krot et al., 2001), and the reasons for chondrule chemical variations given solid precursors (e.g., Sears et al., 1996). The "standard model" in its most basic form holds that chondrule melts behaved as closed systems during their formation and did not chemically interact with the ambient gas. Hence variations in their bulk composition are a result of mixing of precursor solids, possibly nebular condensates, in various combinations (Grossman and Wasson, 1983a,b; Grossman, 1988, 1996; Grossman et al., 1988; Jones and Scott, 1989).

Some variants of the "standard model" suggest that chondrule composition variations were acquired during the chondrule formation event. One such theory supposes that all chondrules had precursors of close to a CI-composition, and during their formation chondrule melts reacted with the ambient gases via evaporation of moderately volatile elements and reduction of iron (Sears et al., 1996; Huang et al., 1996). According to this model, Type II chondrules present a close resemblance to their precursor compositions, which were only slightly modified during the formation event. Type I chondrules on the other hand formed in environments where reduction and/or evaporation were dominant.

Some properties of Type I chondrules may be interpreted as evidence for their formation by open-system melting and hence evaporative loss. Type I chondrules have lower concentrations

* Author to whom correspondence should be addressed (bosmat@rci.rutgers.edu).

of Na, K and S than Type II (e.g., Hewins, 1991). Size measurements of chondrules in Semarkona and Krymka have revealed that the diameter of Type I chondrules are between 15 and 20% smaller than Type II chondrules (Huang et al., 1996). Such a difference in size corresponds to a mass difference of almost 50%, which may be due to evaporation (Sears et al., 1996). Also Type I chondrules contain more metal and silicates with lower FeO relative to Type II. These differences may be attributed to the loss of sulfur from troilite and FeO from silicates due to evaporation.

Hewins et al. (1997) found that nominal grain size in Type I chondrules correlates with their bulk compositions. The concentrations of Na, K, Fe, Ni, P and S decrease as grain size increases. The finest grained chondrules were interpreted as the least melted and therefore considered to be closest to their precursor composition. If compositions were acquired before melting, there would be no a priori reason for the most volatile-rich chondrules to be the most fine-grained (Hewins et al., 1997). Thus these authors concluded that the coarsest grained chondrules have the lowest concentration of moderately volatile elements due to more extensive heating and evaporative loss.

Isotopic mass fractionation is a signature of free evaporation, and one would expect Type II to show less fractionation than Type I if the evaporation discussed by Sears et al. (1996) and Hewins et al. (1997) occurred in the open nebula. Alexander et al. (2000) and Alexander and Grossman (2000) found that chondrule glasses from Bishunpur and Semarkona lack significant potassium isotopic fractionation. Alexander and Wang (2001), Zhu et al. (2001) and Mullane et al. (2003) have measured iron isotope compositions in both Type I and II chondrules and found very small fractionations. Alexander and Wang (2001) concluded that most of their chondrules could not have lost more than 20% of their FeO by Rayleigh evaporation. Because back reaction with K or Fe in the gas could play an important role in evaporation, and suppress isotopic fractionation, extensive iron and potassium loss during the chondrule formation process need not be ruled out. If evaporation occurred in environments with relatively high partial pressures of evaporating elements, extensive back reaction between the gas and chondrules would be likely. Total evaporation of a fine dust fraction to produce high partial pressures of lithophile elements is often discussed as a possible cause of high fO_2 in nebular environments (e.g., Wood, 1985; Wood and Hashimoto, 1993; Rubin et al., 1988; Ebel and Grossman, 2000).

In this study, we tested the open-system melting model for chondrules by heating a CI-like starting material for different lengths of time under canonical-nebula conditions. We expected that during short heating times the starting material would melt and yield Type II chondrule compositions, while over longer evaporation times Type I compositions would form. Experimental charges were analyzed for bulk chemical composition, and for the isotopic and chemical compositions of mineral grains and interstitial glass. Results are compared to properties of natural chondrules.

We also conducted experiments to explore the role of back reaction in suppressing isotopic mass fractionation during evaporation. In these experiments, potassium-rich liquids were heated in semisealed crucibles and cooled at different rates. The charges were analyzed for their chemical compositions and for the isotopic composition of potassium in the glasses. We determined the fraction of potassium lost and the departure of isotopic mass fractionation from Rayleigh fractionation, as a function of cooling rate, to test the evaporation-without-fractionation model of chondrule formation.

Table 1. CI composition from the literature (Anders and Grevesse, 1998) and of the one used in this study (DCP-AES analysis, plus weighed FeS and kerogen) and starting material for K-rich melt experiments (by weighing).

Content in wt.%	Anders and Grevesse* (1989)	CI-like material in this study	K-rich composition
SiO_2	30.58	30.69	52.05
Al_2O_3	2.20	2.56	7.42
TiO_2	0.10	0.06	0.12
FeO	14.57	18.21	4.02
MnO	0.34	0.21	0.07
MgO	21.98	21.35	21.45
CaO	1.74	1.65	10.06
Na_2O	0.90	1.08	0.94
K_2O	0.09	0.14	3.84
FeS	22.32	20.27	0
C	4.66	3.77	0
Total	100	100	99.97

* Normalized to 100%.

2. EXPERIMENTAL METHODS

2.1. Conditions for the Evaporation of CI Material

Experiments were conducted in a DelTech vertical muffle-tube vacuum furnace (Yu et al., 2003). The temperature was monitored using an S type thermocouple ($Pt_{100}/Pt_{90}Rh_{10}$), calibrated against the melting point of palladium (1554 °C). The uncertainty of the temperature measurement is estimated at ±5 °C. An HPS TC61 turbo-pump and an HPS 941 cold cathode pressure gauge were used to monitor the pressure. All experiments were conducted at 1580 °C. When the pressure in the furnace reached 1×10^{-4} torr (1.31×10^{-7} atm), hydrogen gas was introduced into the furnace to a total pressure of 1×10^{-2} torr (1.31×10^{-5} atm).

The composition of the starting material was an anhydrous CI (i.e., solar) mixture (Anders and Grevesse 1989) of minerals calculated to be stable in a vapor of solar composition at 400 K and 10^{-3} bar (Wood and Hashimoto, 1993). At 400 K troilite, a common mineral in chondrules is stable, but water is entirely in the vapor. The mineral mixture included 50 wt.% Kiglapait olivine (Fo_{66}) and 10 wt.% San Carlos olivine (Fo_{88}), which together match the calculated olivine composition, 20.3 wt.% Canyon Diablo troilite (FeS), 3.8 wt.% carbon incorporated as Sarro-Lorraine kerogen and equal amounts (8 wt.%) of diopside and plagioclase, and is shown compared to CI in Table 1. No attempt was made to match Ni. Minerals were crushed to a 45–63 μm powder. The liquidus temperature for the silicate portion of this composition was calculated to be 1633±30 °C following Herzberg (1979).

For each experiment two pressed pellets, between 45 mg and 70 mg, were suspended together on Re-wire loops electro-plated with iron (cf. Lofgren, 1989) and inserted from the antechamber (<250 °C) into the hotspot for 1, 2, 4, 6, 12 and 18 h periods. Charges were quenched by pulling the charges out of the hotspot for an estimated cooling rate of approximately 1000 °C/s.

One of each pair of charges was analyzed on a Direct Current Plasma Atomic Emission Spectrometer (DCP-AES) for bulk composition. Charges, crushed into 200mesh powders, were mixed with $LiBO_2$, fluxed and dissolved in HNO_3 solution. The solutions were run on the DCP-AES together with USGS standards such as BHVO-1, BIR-1 and PCC-1 and working standards. Standards were used for both calibration and as control samples.

The second of each pair of charges was used for phase chemistry analyses of the olivine crystals and mesostasis. These analyses were performed on a JEOL 8600 microprobe using an accelerating potential of 20 kV, a beam current of 15–20 nA. Counting times varied between 20 and 40 s. Sodium and potassium were analyzed first with shorter counting times to minimize loss during analyses. Mesostasis analyses were performed using a 5 μm-rastered beam.

Modal abundances of olivine and mesostasis were calculated using image analysis software. Bulk compositions obtained from phase compositions, modal abundances and densities for glass and olivine at different temperatures (Herzberg, 1987) were overall in agreement with bulk compositions determined by DCP-AES. However, there are some discrepancies in concentrations of FeO in the long heating runs. Wire was analyzed for Fe by electron microscope.

Silicon isotopic analyses were performed using a Cameca IMS 6f ion probe at Carnegie Institution of Washington at mass resolution of 5500. Operating conditions were 12.5 kV O^- primary beam and 10 kV secondary acceleration voltage with a 50eV energy window. Repeated analyses gave a standard deviation of about 1‰ for δ^{29}Si and δ^{30}Si. The primary standard was BHVO basaltic glass (Govindaraju, 1994).

2.2. Conditions for K-Evaporation Experiments

Experiments were conducted in a DelTech vertical muffle-tube vacuum furnace (Yu et al., 2003). Since the purpose of these experiments was to study the isotopic mass fractionation of K, we chose a starting material with a relatively high K-content. It consisted of 40% diopside, 30% microcline and 30% San Carlos olivine. Oxide composition is shown in Table 1.

A pressed pellet made of 57–58 mg of starting material was placed on a molybdenum twisted coil, which was suspended inside a hand-molded Mo crucible. The crucible was then covered with molybdenum foil. The foil was hand tightened to the rim of the crucible. Experiments were conducted at 1380 °C, which is about 15 °C below the liquidus temperature of the starting material. When the pressure in the furnace reached 1×10^{-6} torr (1.31×10^{-9} atm), hydrogen gas was introduced into the furnace to a total pressure of 1×10^{-4} torr (1.31×10^{-7} atm). At the start of the experiment, the hydrogen flow was turned off and the valve connecting the muffle tube and the pump was closed. At this point the sample was lowered into the hot spot of the furnace. Each sample was first held at 1380 °C for 20 min and then cooled at different cooling rates (10, 50, 100, 1000, 5000 °C/h) to 400 °C. Run times were ~20 min to ~100 h.

Experimental residues were analyzed on a JEOL 8600 microprobe, using an accelerating potential of 15 kV and a beam current of 15–20 nA. To prevent K loss during analyses, counting times were 2–5 s using a rastered beam of ~5 μm.

The K-isotope analyses were performed exactly as for Si. Repeated analyses of the BHVO standard gave a standard deviation of about 1‰ for δ^{41}K.

3. RESULTS

3.1. Results from CI Evaporation Experiments

3.1.1. Chemical composition of evaporative residues

The experimental charges consisted of only two phases, porphyritic olivine in glass (which contained some olivine quench crystals). Back-scattered electron images (Fig. 1) and optical examination of the recovered charges show no sulfides or metallic iron in any of them. Bulk compositions of the 6 experimental residues produced by 1, 2, 4, 6, 12 and 18 h of heating are presented in Table 2. Potassium, sodium and troilite are undetectable after 1 h of evaporation, consistent with Yu et al. (2003). FeO contents (moles) increase, relative to initial material, after 1 h of heating. This increase must result from oxidation of FeS by oxygen probably from Na_2O and K_2O decomposition, or from oxygen present in the vacuum furnace itself. Oxidation of iron under relatively reducing conditions has been observed in several previous studies (e.g., Hashimoto, 1983; Wang et al., 2001) but not associated with loss of alkalis. A calculated 1.36 wt.% of FeO was produced in this way in the first hour. We corrected for this gain in calculating the loss of FeO from the starting material in the results reported below.

Although DCP-AES and electron probe results are similar, DCP-AES analyses were performed on whole charges. They are assumed to be more representative of the bulk composition and are therefore preferred in the discussion below.

The masses of charges analyzed by DCP-AES before and after heating are shown in Table 2 and were calculated under the assumption that the Al_2O_3 content in each charge remained constant during heating (Hashimoto, 1983). Weight-losses increase gradually with heating times. In Figure 2 we plot the concentrations of oxides versus fraction of initial mass remaining (the residual fraction). The fraction lost in the first hour (~25 wt.%) consisted mostly of FeS, C and alkalis. After the complete loss of FeS, FeO becomes the major evaporating component, and is almost entirely lost after 6 to 12 h of heating. After 6 h of heating, SiO_2 is the major evaporating species. The evaporation of MgO becomes significant only after 12 h of heating. This evaporation sequence is consistent with earlier results (e.g., Hashimoto, 1983; Nagahara and Ozawa, 1994; Floss et al., 1996; Wang et al., 2001).

In Table 3, we present the compositions of olivine and mesostasis in the different experimental runs. Olivine grains become progressively more forsterite-rich, going from Fo_{70} on average in the starting material to Fo_{82} after 1 h, to Fo_{99} after 12 h of heating. Similar trends were observed in olivine bearing residues by Floss et al. (1996). The big change in the first hour is probably related to partial melting as the Kiglapait olivine has been heated to near its solidus temperature. Subsequent changes in olivine composition are primarily due to evaporation from the melt. Glasses become more Fe-poor and Ca- and Al-rich with time.

The volume percentage of olivine grains increases from an average of 43% in charges heated for 1–6 h to 68% for 12–18 h (Fig. 3). Olivine also coarsens, from 100μm across after 1 h to several hundred μm after 12 h. This gives rise to a zonation in some grains in these isothermal runs: cores of "relict" olivine with compositions modified by exchange with the melt are mantled by melt-grown olivine because of the Ostwald ripening process. Some olivine grains are zoned with respect to MgO and FeO or CaO and Al_2O_3. MgO and FeO zoning is observed mainly in the 4- and 6-h runs, though rare "relicts" are found in longer runs (Fig. 4). CaO zoning is weak or absent in the shorter runs, but strong in the 12- and 18-h runs. In the 4- and 6-h runs, the amount of MgO increased towards the rims by 3 and 5 wt.%, respectively, relative to the center of the grain, and FeO decreased toward the rims by a similar amount. Zoning of CaO was steeper, with CaO increasing from 0.1 wt.% to about 0.15 wt.% in the 6-h run and up to 0.9 wt.% in the 18-h run (Fig. 4).

The Re-wires supporting the charges contain decreasing amounts of iron as heating time increased. In the two longest runs, no iron was detected in the wires. Since the wires were iron-plated before the experiments, we do not believe that any iron from our samples was lost to the wires. Any iron gain by

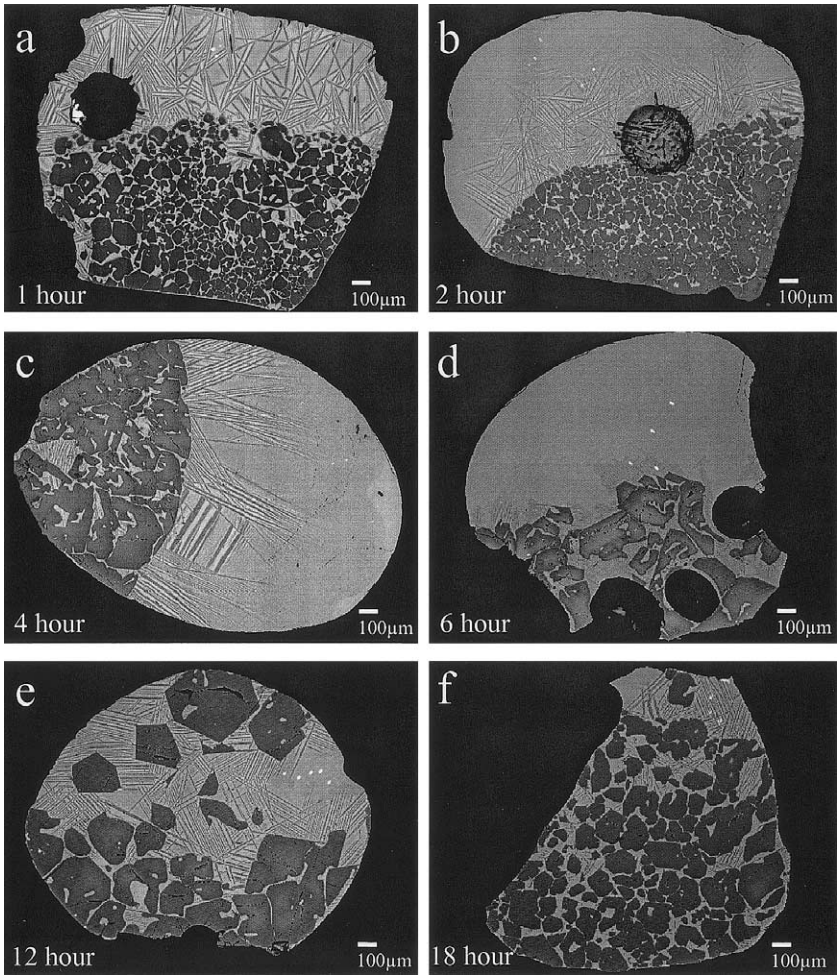

Fig. 1. Back scattered scanning electron microscope images of the experimental residues, showing olivine and mesostasis.

the samples from the wires is likely to be very small, given that large quantities of Fe derived from troilite were lost by evaporation. It is probable that Fe was lost from the wires by evaporation.

3.1.2. Evaporation rate constants

Evaporation rate constants for FeO, SiO_2 and MgO were calculated using the formulae in Tsuchiyama et al. (1981). The

Table 2. Volatile-free starting composition and composition of experimental charges analyzed by DCP-AES. Weights are given in mg. Liquidus temperatures calculated after Herzberg (1979).

Oxide (wt.%)	CI[†]	1 h	2 h	4 h	6 h	12 h	18 h
SiO_2	40.34	40.19	41.68	45.49	47.25	41.76	38.66
Al_2O_3	3.36	3.35	3.64	4.16	4.63	5.96	7.67
TiO_2	0.08	0.09	0.08	0.10	0.11	0.12	0.16
FeO	25.72	24.90	21.17	12.87	3.61	0.96	1.2
MnO	0.28	0.20	0.19	0.14	0.07	0.02	0.02
MgO	28.05	28.62	30.43	34.61	40.7	46.75	46.56
CaO	2.17	2.24	2.37	2.60	3.10	3.91	4.87
Liquidus (°C)	1633	1640	1646	1661	1702	1775	1782
Weight initial[‡]		59.9	56.6	63.4	70.4	74.5	70.0
Weight final		44.64	39.73	38.99	38.87	31.98	23.34
Weight loss (%)		25.47	29.80	38.51	44.79	57.08	66.66

[†] CI composition calculated by normalizing the composition in Table 1 to 74.73 wt.% (residue after loss of FeS, kerogen and alkalies in the first hour) and adding 1.36 wt.% to FeO, produced by oxidation of Fe from FeS.

[‡] Weights were calculated assuming no loss of Al.

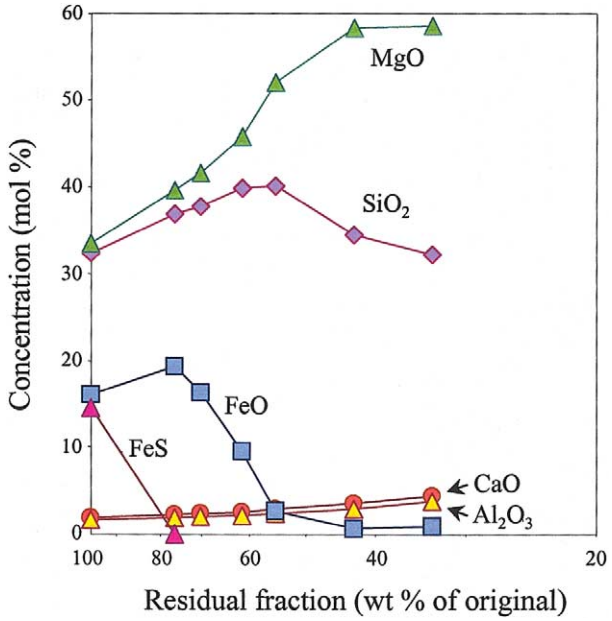

Fig. 2. Concentrations (in mole%) of FeS, FeO, SiO_2, MgO, CaO and Al_2O_3 as a function of the residual mass fraction of the charge (wt.%).

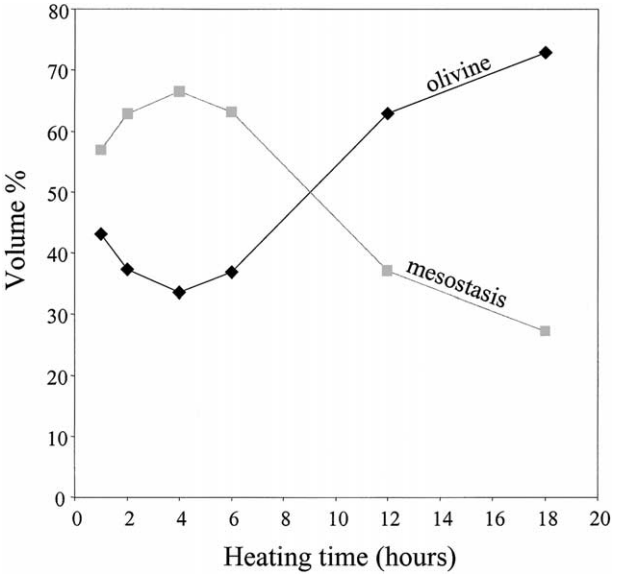

Fig. 3. Volume percent of olivine and mesostasis in experimental charges.

evaporation flux, J_i (mole/min), of each species *i* from the melt, is equal to:

$$J_i = k_i A C_i \quad (1)$$

where *A* is the surface area of the liquid sphere, C_i (mole/cm^3) is the concentration of the species *i* in the liquid and k_i is the evaporation rate constant (cm/min). Assuming that the activity coefficients of all species in the melt for species *i* are constant,

$$ln\left(C_i/C_{i,o}\right) = -3k_i t/r \quad (2)$$

(Tsuchiyama et al., 1981) where *r* is the radius of the sphere. The average radii of the pellets, although they decreased slightly with time, are taken to be $r = 0.15$ cm. Table 4 shows

Table 3. Final compositions of olivine, mesostasis, isotopic composition of silicon in mesostasis (δ^{29}Si and δ^{30}Si error in parenthesis) and calculated FeO evaporation rate (J) in the experimental charges.

Oxide (wt.%)	1 hr	s.d.*	2 h	4 h	6 h	12 h	18 h
Olivine							
No. of analyses	19		16	21	17	15	16
SiO_2	38.48	0.50	39.47	40.68	41.99	42.66	42.55
Al_2O_3	0.02	0.051	0.03	0.02	0.03	0.07	0.32
TiO_2	0.03	0.019	0.00	0.01	0.01	0.01	0.02
FeO	16.79	0.63	15.81	10.65	4.73	0.60	0.33
MnO	0.21	0.019	0.05	0.07	0.06	0.01	0.00
MgO	43.56	0.63	44.19	47.95	52.84	55.62	55.51
CaO	0.13	0.066	0.14	0.09	0.12	0.25	0.64
Total	99.21		99.69	99.47	99.77	99.23	99.38
Fo content	82.22		83.28	88.92	95.22	99.40	99.66
Mesostasis							
No. of analyses	13		14	11	12	14	10
SiO_2	44.69	1.51	45.63	48.98	52.42	45.50	37.62
Al_2O_3	5.46	0.044	5.44	4.84	7.02	14.26	17.18
TiO_2	0.11	1.75	0.11	0.10	0.15	0.29	0.42
FeO	25.95	0.92	21.74	13.19	2.20	0.11	0.02
MnO	0.24	0.027	0.20	0.14	0.06	0.01	0.00
MgO	19.64	6.00	21.82	28.07	31.21	29.15	26.69
CaO	4.08	1.97	4.03	3.96	5.84	10.96	17.90
Total	100.14		99.00	99.32	98.92	100.31	99.85
δ^{29}Si (‰)	0.57 (0.37)		1.44 (0.33)	3.37 (0.35)	NA	10.02 (0.48)	13.88 (0.47)
δ^{30}Si (‰)	1.71 (0.54)		2.12 (0.48)	6.39 (0.53)	NA	18.99 (0.59)	26.96 (0.65)
J (mole/cm^2/s)	3.94×10^{-6}		2.82×10^{-5}	2.38×10^{-5}	2.02×10^{-5}	1.80×10^{-6}	1.17×10^{-8}

* Averaged standard deviations.
NA: not analyzed.

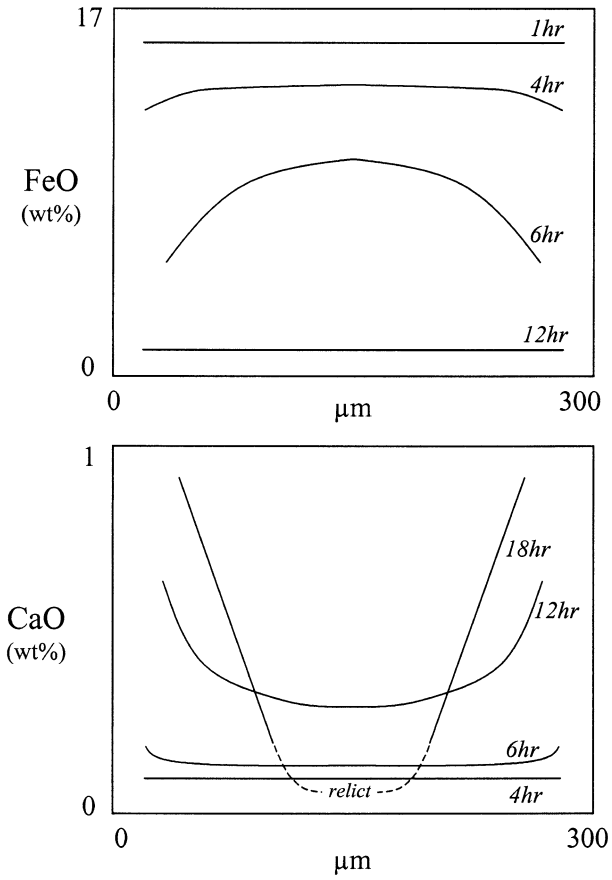

Fig. 4. A schematic illustration of the zoning profiles of FeO (wt.%) and CaO (wt.%) in the olivine grains in the different evaporation runs.

the evaporation rate constants for FeO, SiO_2 and MgO, calculated from the slopes, $-3k_i/r$, of plots of $ln(C_i/C_{i,o})$ versus t (Fig. 5).

3.1.3. Silicon isotopic composition

Silicon isotopic compositions ($^{29}Si/^{28}Si$ and $^{30}Si/^{28}Si$ in parts per thousand relative to the BHVO basaltic glass standard, Table 3) of run product glasses are plotted against $-\ln[(Si/Al)/(Si/Al)_o]$ in Figure 6. The Si/Al ratios in Figure 6 are normalized to the Si/Al ratio in the mesostasis from the 1-h run.

The quenched liquid in the charges consists of glass plus olivine dendrites. The data for the mesostasis in our evaporation residues describe unusual trajectories in Figure 6, because both evaporation and crystal-liquid interaction occur during the experiment, as discussed in section 4.4. However, despite these

Table 4. Calculated evaporation rate constant, k, at 1580 °C and 1.31×10^{-5} atm.

Oxide	k (cm/min)
FeO	2.65×10^{-4}
SiO_2	4.0×10^{-5}
MgO	1.0×10^{-5}

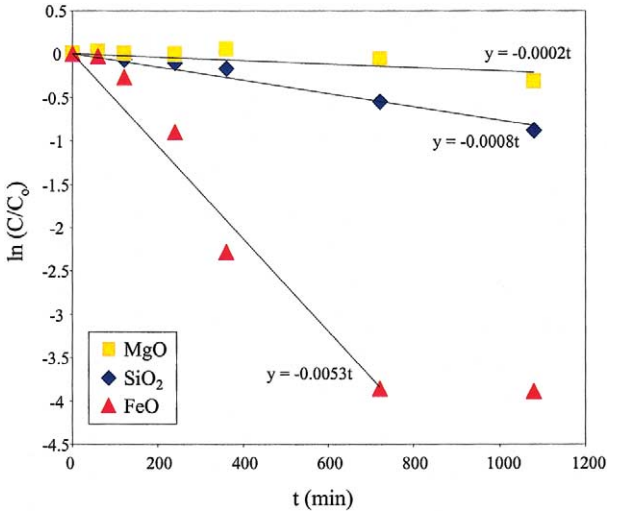

Fig. 5. Natural log of the bulk concentration of FeO, SiO_2 and MgO normalized to starting composition (mole fraction) in experimental residues vs. heating time (minutes).

complexities, the melt in the long duration runs shows close to the expected Rayleigh fractionations.

3.2. Results from Evaporation Experiments of Potassium-Rich Melts

The mineral assemblage in the charges depended on cooling rate. It consisted of olivine and glass for higher cooling rates, but the charges recovered from the 50 °C/h and 10 °C/h cooling runs contained diopside in addition to olivine and glass. Olivine crystals were usually 10–30 μm and consisted mostly of San Carlos relicts. Grain sizes increased with lower cooling rates.

The concentration of potassium in the charges decreased with decreasing cooling rates (Table 5 and Fig. 7). The K/K_o

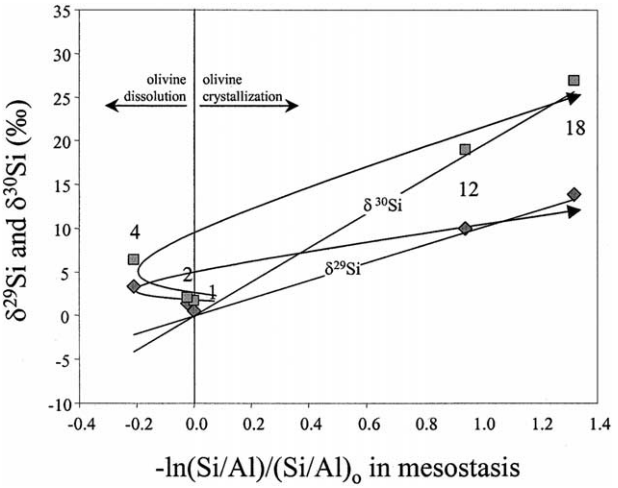

Fig. 6. $\delta^{29}Si$ and $\delta^{30}Si$ (‰) measured in the mesostases versus $-\ln[(Si/Al/(Si/Al)_o]$ in the mesostases from the evaporation residues of 1, 2, 4, 12 and 18 h. Solid lines are fit to the 12 and 18-h runs and are used to calculate alphas. Curved arrows follow the evaporation trend (hand drawn).

Table 5. K/K_o ratios, $\delta^{41}K$ (actual and calculated rayleigh values) in the mesostases, and Fo content of the olivines.

Cooling rate (°C/h)	K/K_o	$\delta^{41}K$ (‰)	err.	Rayleigh	Fo
5000	0.45	8.47	0.84	19.69	80.3
1000	0.39	18.67	0.71	23.25	84.1
500	0.34	13.97	0.90	26.52	85.1
100	0.12	42.71	0.72	53.05	86.6
50	0.021	75.50	1.14	95.02	88.2
10	0.002	66.50	5.99	161.7	88.0

ratios decreased from 0.45 wt.% for the fastest cooling rate experiment to ~0.002 wt.% for the slowest and follow a logarithmic law in agreement with (Xiong and Hewins (2003). The magnesium content in the olivine grains increased as cooling rates decreased due to the evaporation of iron (Table 5), from Fo_{80} in the 5000 °C/h up to about Fo_{88} in the 10 °C/h run.

Measured values of $\delta^{41}K$ in the mesostases of the different charges are shown in Table 5 and Figure 8. Also shown are the Rayleigh mass fractionation values (calculated from $\ln(K/K_o)\times 1000$) expected during free evaporation. As cooling rates decreased the amount of isotopic mass fractionation increased. However, the $\delta^{41}K$ values measured in the charges all fall below the Rayleigh fractionation line with deviations from the expected values increasing as cooling rates decrease (Fig. 8). In the lowest cooling rate experiment (10 °C/h), the measured mass fractionation was lower than the one at 50 °C/h, even though the amount of potassium lost was higher.

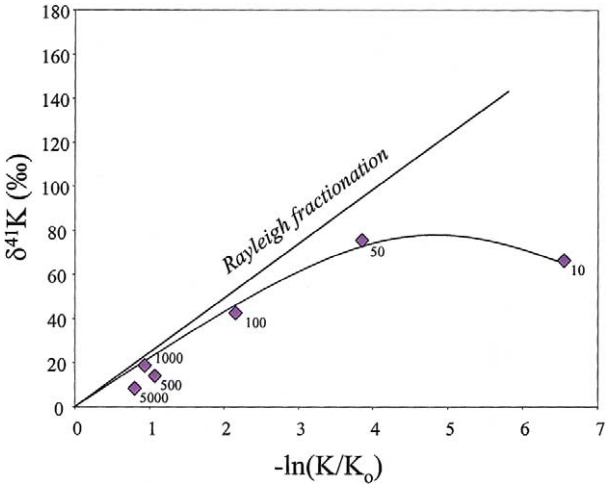

Fig. 8. Isotopic mass fractionation of K as a function of fraction of K retained in residue. The expected Rayleigh mass fractionation line is also shown. Marked numbers are cooling rates (°C/h). Due to back reaction between the gas and the melt, isotopic fractionation is partially suppressed. This effect becomes more pronounced as cooling rates decrease. Hand drawn line between the experimental values for emphasis.

4. DISCUSSION

4.1. Experimental Residues and Natural Chondrules

The FeO and SiO_2 contents in the bulk experimental residues are compared to the bulk compositions of Semarkona chondrules (from Jones and Scott, 1989; Jones, 1990, 1994, 1996) in Figure 9. The evaporation trend defined by our experimental charges matches, after some FeO loss, the compositions of most Type IIA and, after additional FeO and SiO_2 loss, most Type IA chondrules. The compositions of the silica-rich Type IB and IIB chondrules fall to the right of the evaporation trend and are not reproduced in our experiments. On a portion of the MgO-SiO_2-FeO ternary diagram (Fig. 10), the experimental residues also coincide with the compositions of most silica-poor Type IIA and IA chondrules, but not Type B chondrules.

The observed shift of residues to more refractory bulk compositions is also evident in the abundance and composition of the olivine grains. The abundance of olivine decreases as FeO is lost (0–6 h), and increases again as SiO_2 is lost (6–18 h), as shown in Figure 3. The composition of the olivine increases from Fo_{82} after 1 h to Fo_{99} after 12 h of heating, as the bulk

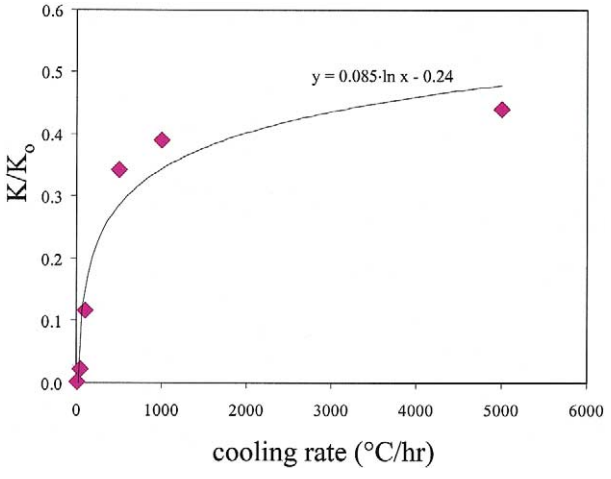

Fig. 7. Fraction of K retained in charge as a function of cooling rate. The change in K/K_o as a function of cooling rate follows a logarithmic law (curve).

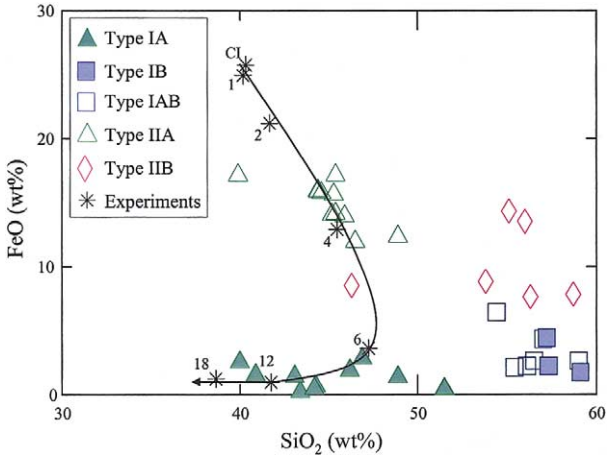

Fig. 9. FeO vs. SiO_2 in wt.% in Semarkona chondrules (Jones and Scott; 1989; Jones, 1990, 1994, 1996) and in the experimental residues. Curved arrow represents the evaporation trend. Numbers near stars indicate heating time in each experiment.

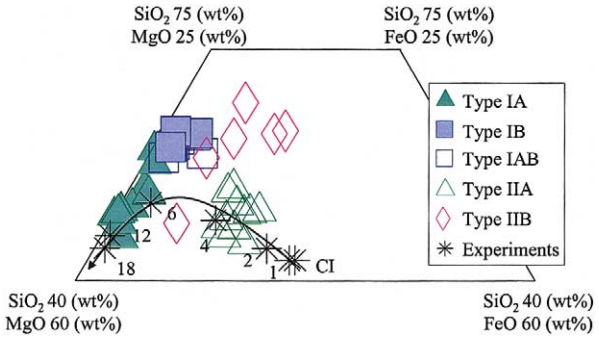

Fig. 10. A SiO_2, FeO and MgO ternary diagram showing the compositions of the experimental residues and of natural chondrules (wt.%). CI represents the starting material used in the experiments. Curved arrow represents the evaporation trend. Numbers near stars indicate heating time in each experiment.

composition becomes more MgO+SiO_2 rich due to FeO loss (Fig. 11a, Table 3). This correlation between bulk composition and the composition of olivine grains is observed in natural chondrules (Jones and Scott, 1989; Jones, 1990, 1994, 1996) of all chondrule types (Fig. 11a).

In our experiments, as molar Mg in the olivine grains (X_{Fo}) increased (due to evaporation) the CaO and Al_2O_3 content (wt.%) of the olivines increased as well (Table 3). This forsterite-calcium correlation (Fig. 11b) is also observed in natural chondrules of all compositions (Scott and Taylor, 1983; Jones and Scott, 1989; Jones, 1990, 1994, 1996). Furthermore, as the CaO wt.% in the olivines increased, the CaO in the mesostasis increased as well (Fig. 11c and Table 3). Ca partitioning between olivine and melt is discussed below. The resemblance between olivine composition in chondrules and the evaporative residues, regardless of chondrule bulk MgO/SiO_2 ratios which may result from precursor variations, suggests that enrichment in Mg and refractories in all these liquids is due to evaporation of FeO.

In the current experiments, many chondrule chemical compositions were reproduced by iron and silica loss from a CI-like parent, but silica-rich chondrules were not. One way to explain silica-rich (Type B) chondrules is that their precursors were more silica-rich relative to CI or the precursors of Type As. Upon moderate heating such precursors would have lost a little FeO to give rise to Type IIB and upon more intensive heating and substantial loss of FeO would have generated Type IB. To demonstrate this, we chose a composition Q, which has a higher SiO_2 content relative to CI (Fig. 12) and calculated its evaporation path, using the evaporation rate constants (k) of FeO, SiO_2 and MgO determined above (assuming k is not composition dependent). Evaporative residues of precursor Q match after short heating times Type IIB compositions and after 12 and 18 h Type IB compositions (Fig. 12). In fact, as can be seen in Figure 12, any composition that plots along the arrow can produce a number of chondrule compositions upon evaporation. If chondrules formed by open-system melting, their precursors included several compositions of varying SiO_2 content.

Several origins have been proposed for Type B chondrules, such as fractional condensation in highly dust-enriched domains, with formation of orthopyroxene-liquid assemblages after removal of large quantities of olivine (Ebel et al., 2003) or recondensation of silica during late stages of chondrule formation (Matsunami et al., 1993; Tissandier et al., 2002). However, Alexander (1994, 1996) suggested that Type B chondrules were formed through the recycling of silica-rich glass separated from chondrules and rims enriched in SiO_2 that was evaporated from chondrules. If silica-rich glasses and rims were in fact separated from previous generations of chondrules and mixed back with a CI average composition then this may provide the mechanism

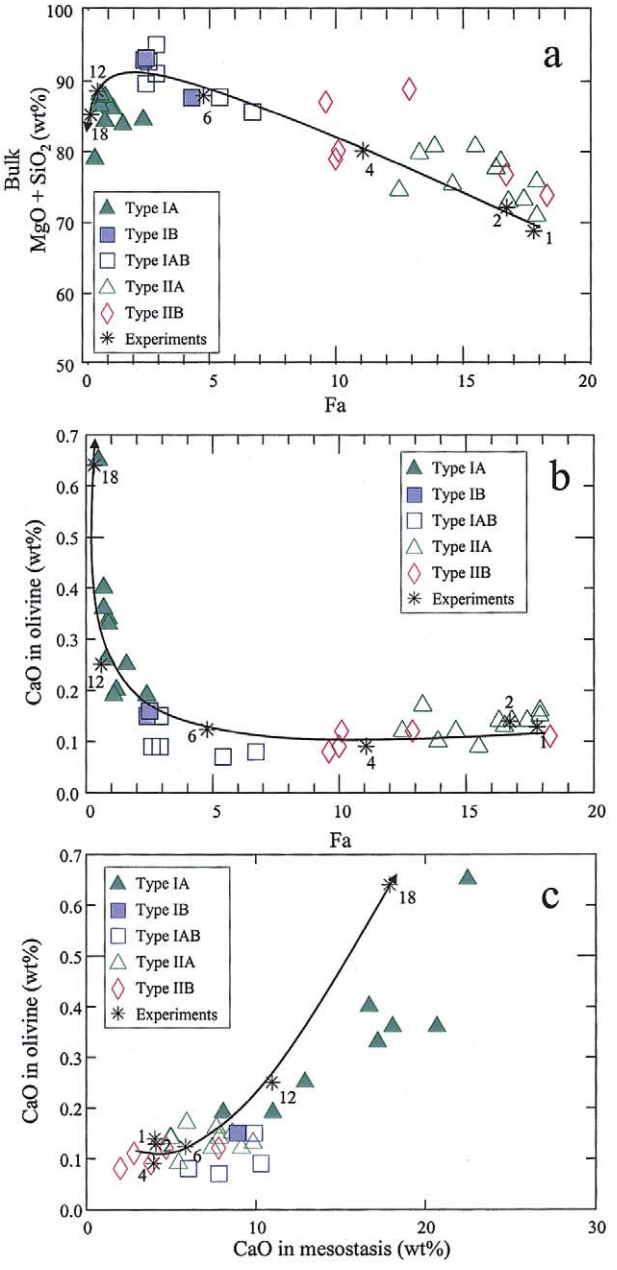

Fig. 11. Analyses of experimental charges and Semarkona chondrules (Jones and Scott, 1989; Jones, 1990, 1994, 1996). a. Bulk SiO_2 +MgO (wt.%) versus fayalite content in olivine. b. CaO in olivine versus fayalite content in olivines. c. CaO content in olivine versus CaO content in the mesostasis. Curved arrow represents the evaporation trend. Numbers near stars indicate heating time in each experiment.

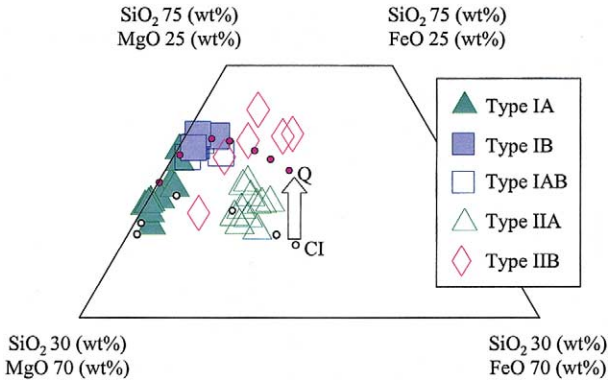

Fig. 12. Evaporation trends for a CI starting material (open circles) from experiments and a potential starting material Q (solid circles), calculated from the experimentally determined evaporation rate constants. CI starting material can produce Type IA and IIA chondrules by open-system melting. Type IB and IIB chondrules may have formed by the evaporation of a more pyroxene-rich precursor such as composition Q. Any composition that plots along the arrow (pointing to increasing SiO_2/(MgO+FeO) ratio) can produce a range of intermediate chondrule compositions upon evaporation.

for making the spectrum of precursors needed to produce all chondrule types by open-system melting.

4.2. Formation Times for Chondrules

The evaporation experiments of CI material were conducted under conditions similar to those generally assumed for the canonical nebula in which chondrules are believed to have formed. Using the experimentally determined evaporation rate constant for FeO allows us to estimate chondrule formation times. Eqn. 3 relates the change in concentration, due to evaporation, to heating time through the slope, $-3k/r$ (0.0053 in our experiments for FeO). The experimental charges have a radius of 1.5 mm, three times that of average chondrules (Scott et al., 1996), therefore

$$t = ln\left(C/C_o\right)/(3 \times 0.0053) \quad (3)$$

gives the formation time for average chondrules under the conditions of the experiments.

Since the initial masses of chondrules are unknown, the average weight percent values of FeO, SiO_2 and MgO in the different chondrule types (Jones and Scott, 1989; Jones, 1990, 1994, 1996), which were used to substitute for C, were normalized to the average Al_2O_3 (wt.%) in each chondrule type.

C_o for FeO, MgO and SiO_2 were taken from three potential starting compositions: CI, Semarkona (Jarosewich, 1990) and Type IIA chondrules (Jones, 1990), all normalized to their respective Al_2O_3 contents. Calculated formation times for the different chondrule types are presented in Table 6 and in Figure 13a–c, and vary depending on the choice of starting composition, but display a rather narrow range. If chondrules formed by evaporation with $P_{H2} \sim 10^{-5}$ atm, as in our experiments, then Type II chondrules were hot for at least 0–0.65 h and Type IA chondrules for at least 3.1–3.7 h. If chondrules formed at $P_{H2} \cong 10^{-3}$ atm, their heating times could be an order of magnitude shorter, because of the strong dependence of evaporation rates on P_{H2} in the hydrogen reaction regime (Nagahara and Ozawa, 1996; Tsuchiyama et al., 1999; Kuroda and Hashimoto, 2002; Richter et al., 2002). However, if chondrules formed in domains with high partial pressures of the elements of interest, because of dust evaporation, the heating times would have been longer.

These results provide an interesting insight into the origin of the near or even super-chondritic levels of volatile elements, such as Fe, S and Na, in Type II chondrules. If Type II chondrule precursors contained volatiles and were subsequently heated for up to 0.65 h in the canonical nebula, they would not have preserved any volatiles either. Therefore, volatiles found in Type II chondrules, or on rare occasions in Type I, cannot be primary in origin if these chondrules formed in the canonical nebula, and must have been introduced into chondrules during or after cooling. Alternatively, if chondrules were heated in nebular domains with high partial pressures of lithophile elements (Wood, 1985; Alexander et al., 2000; Desch and Connolly, 2002; Yu et al., 2003), then alkalis etc. found in chondrules could be primary.

4.3. Ca-Rich Olivines: Experimental vs. Natural

Weinbruch et al. (2000) have suggested that isolated Ca-rich forsterite grains (refractory forsterite) in primitive meteorites are the result of condensation. Such grains are also found in refractory chondrules (McSween, 1977b; Jones, 1992; Steele, 1986; Alexander, 1994). In this study we crystallized similar Ca-rich forsteritic olivines in a melt during evaporation. Olivines from the 1–6 h runs (CaO = 0.1–0.2 wt.%) match the Fo and CaO content of olivines in Type IIA, IIB, and IAB chondrules (Fig. 11b) and experiments of 12–18 h produced olivine grains (CaO = 0.25 and 0.65 wt.%) matching olivines in Type IA (Fig. 11b). These values also overlap the CaO content in refractory forsterites from Allende (Weinbruch et al., 2000). The CaO content of olivines and surrounding glass are correlated in both the experimental residues and natural chondrules (Fig. 11c). The longest duration runs show strong Ca zoning in olivine.

Libourel (1999) devised a method, which removed the bulk composition and temperature controls on the distribution of CaO between olivine and liquid, for a vast array of terrestrial rocks and experimental charges, and allowed the partition coefficient to be expressed as a function only of the Fo content of the olivine. CaO partition coefficients for natural chondrules

Table 6. The calculated heating times (in hours) for producing different chondrule types if they formed by evaporation of FeO from three different precursors. The times were calculated using the evaporation constants given in Table 4 assuming an initial radius of 0.5 mm. These times only apply to the conditions at which the evaporation constants were measured.

Precursor Chondrule	Semarkona	CI	Type IIA Chondrules
Type IIA	0.65	0.2	0
Type IIB	1.3	0.9	0.7
Type IAB	2.2	1.6	1.4
Type IB	2.3	1.8	1.6
Type IA	3.7	3.2	3.1

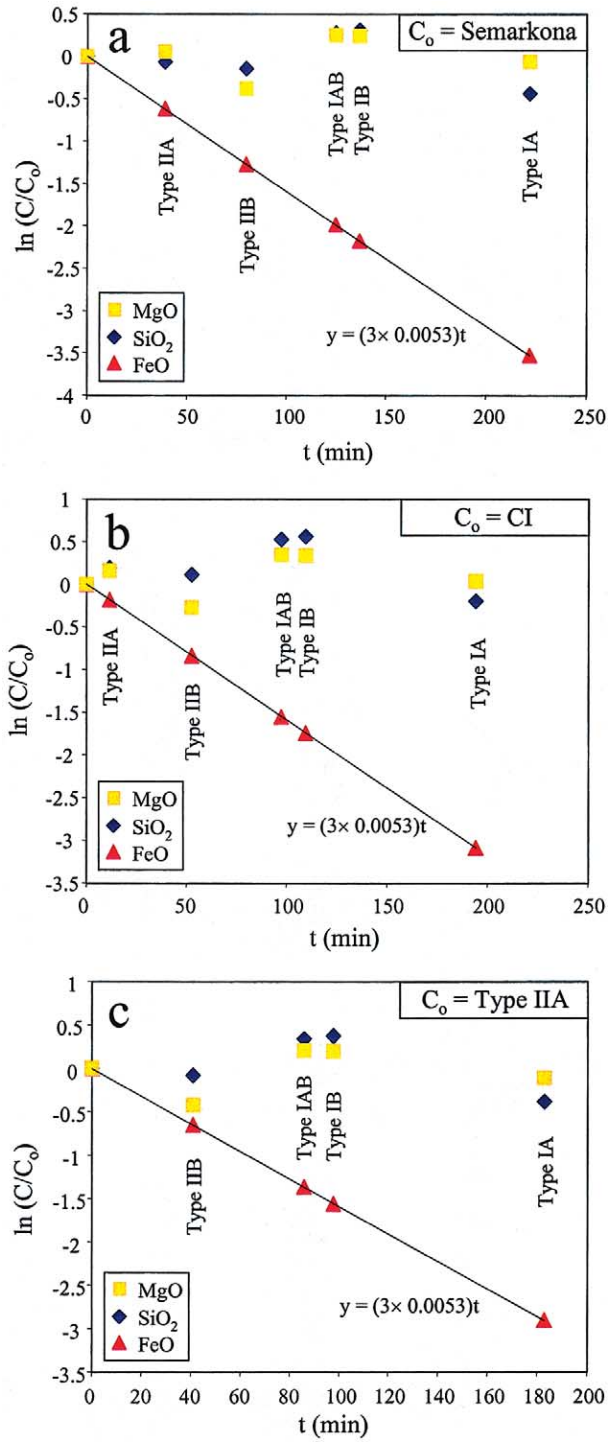

Fig. 13. The change in composition of chondrules with time (red triangles) compared to the bulk composition of Semarkona chondrules (Jones and Scott, 1989; Jones, 1990, 1994, 1996). The average FeO, SiO_2 and MgO from the different chondrule types are normalized to Al_2O_3 and three precursor compositions: a. CI. b. Semarkona. c. Type IIA. Heating times (t) were calculated based on the experimentally determined evaporation rate for FeO at 1580 °C.

(Fig. 14a) and for experimental residues (Fig. 14b) were calculated using the simplification devised by Libourel (1999):

$$D_{CaO}^{ol\text{-}melt} = X_{CaO}^{ol} / a_{CaO}^{melt} \quad (4)$$

where D is the Ca partition coefficient, X_{CaO}^{ol} = CaO/(CaO + MgO) in olivine (mole fraction), and a_{CaO}^{melt} is the pseudoactivity of CaO in the melt and in the absence of alkalis is given by:

$$a_{CaO}^{melt} = (X_{CaO}^{melt})^2 / (X_{SiO2}^{melt} + X_{TiO2}^{melt}) \quad (5)$$

where X^{melt}_i is the mole fraction of oxide *i* in the melt. The CaO wt.% in the olivine grains from 1- through 6-h runs was usually uniform. In the 12- and 18-h runs the olivine rims grains were enriched in CaO relative to their centers and we calculated D using an average CaO value from the rims since they were the last to be in contact with the current mesostasis. The solid lines shown in Figure 14a,b represent the partition coefficients of CaO between olivine and melts as a function of forsterite content under equilibrium conditions determined empirically by Libourel (1999) by fitting a large body of data to obtain the equation:

$$\ln D = -1.24X_{Fo}^3 + 3.33X_{Fo}^2 - 6.55X_{Fo} + 2.05 \quad (6)$$

Comparing CaO partition coefficients of natural chondrules and our experiments with the Libourel (1999) curve can serve

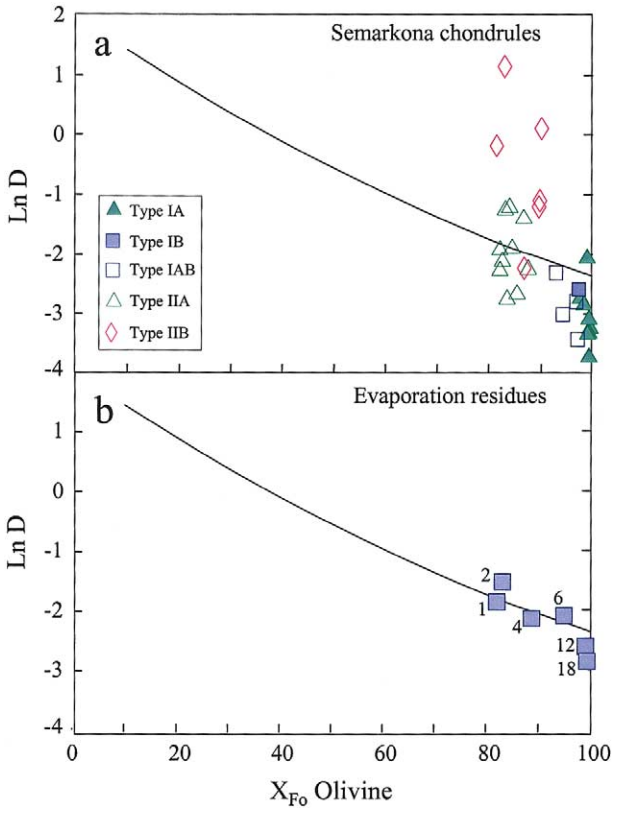

Fig. 14. (a) Partition coefficients (ln D) of CaO between olivine and melt vs. forsterite content of olivine in Semarkona chondrules (Jones and Scott, 1989; Jones, 1990, 1994, 1996). Solid line represents equilibrium partitioning of CaO calculated by Libourel (1999). (b) Results from experimental residues.

as a test for equilibrium. Figure 14a shows that most Type IIA chondrules cluster around the equilibrium line, while Type IIB spread above the line and Type IA, IAB and some IIA spread below it exhibiting disequilibrium with respect to CaO partitioning. Residues from the 1–6 h runs lie on the equilibrium line (Fig. 14b), whereas the 12- and 18-h runs, due to a lower CaO content in olivine relative to that in the melt, show disequilibrium with respect to CaO partitioning and overlap Type IA chondrules.

The CaO content of the olivines in the starting material averages 0.06 wt.% (0.03 and 0.18 in Kiglapait and the San Carlos olivines, respectively). The CaO contents of the olivines in the experimental charges of 1, 2, 4 and 6 h average 0.12 (total range 0.06 to 0.17 wt.%) with no significant variation between core and rim of grain, or from charge to charge. Thus CaO contents in the olivines from the first 6 h of evaporation are different from the average CaO content in the starting material. A possible interpretation of the results shown in Figure 14 is that the olivines of the 1 to 6 h runs and some Type IIA olivines were able to reach equilibrium in CaO between olivine and melt, even though they were heated for relatively short durations. This occurred mostly because the CaO contents of relict grains of the starting material (the more refractory San Carlos olivines) were not much different from the composition in equilibrium with the initial melts, and because the concentration of CaO in the late melts due to evaporative loss of FeO was not severe.

The evaporative loss of iron and silicon from the melt was faster than the rate of Ca redistribution between the melt and the olivine in the 12 and 18-h runs. Their olivine grains have higher CaO contents in their cores (0.25 and 0.51 wt.% with a s.d. of 0.27 and 0.06 for 12 and 18 h respectively) than those in the shorter runs and even more CaO-rich zoned rims (up to 1.0 wt.%). The strong zonation reflects the inability of Ca to diffuse into the olivine fast enough to keep pace with changing liquid composition when SiO_2 loss is important. With a diffusion coefficient for Ca of about 10^{-10} at this temperature (Jurewicz and Watson, 1988), the time required to produce half the equilibrium concentration at 10 μm from the rim is about 3 h (Köhler and Brey, 1990) whereas our olivine grains are several hundred μm across. However, as the CaO concentration of the liquid is continually increasing due to evaporation, a precise diffusion calculation cannot be done.

Type IA and IAB chondrules, and our experimental runs of 12 and 18 h, display disequilibrium with respect to Ca (Fig. 14). These chondrules probably experienced longer heating times than Type IIA chondrules and consequently a higher evaporation loss of iron and silicon. The array of Type IIB chondrules lying above the equilibrium line has no experimental analogues, perhaps reflecting dilution of the Ca in the liquid rather than concentration. This might have been achieved by condensation of Si and/or Fe into the chondrule melt. The greater spread of chondrules relative to the run products may be related to the fact that only the edge of the olivine crystal would have been near equilibrium with the mesostasis and some of the data shown may represent crystal centers. The experimental data show a much closer approach to equilibrium than the natural chondrules, which is not surprising as we have heated isothermally for long durations and then quenched. The only systematic deviation from Libourel's curve is for the longest runs, which suffered the greatest evaporative losses. Here we used olivine rim compositions, as the core compositions, little modified by diffusion during evaporation of the liquid, would give even lower partition coefficients. Natural chondrules may not give equilibrium partition coefficients for a variety of reasons: they experienced fractional crystallization such that olivine cores were not in equilibrium with the late liquid represented by mesostasis; relict grains may be included in the olivines analyzed; the liquid may have been modified by evaporation or condensation during crystallization; the glass may have been modified by alteration with leaching of Ca. Some of these effects might be expected to influence all kinds of chondrules equally, but Figure 14a shows that type I chondrules tend to have low D values whereas D for Type II chondrules can be higher than the equilibrium value. We suggest that the low Ca partition coefficients for Type I chondrules reflect Ca enrichment of late chondrule melts by evaporative loss of FeO and SiO_2. The higher values for Type II chondrules might reflect the absence of evaporation, with the large ranges explained by a combination of the other effects noted above. The systematically high D values for Type IIB chondrules are for small olivine grains poikilitically enclosed by pyroxene. They might be explained by dilution of Ca in the melt by condensation of Si and/or Fe.

We have shown that Ca-rich olivines, comparable to those in Type I and refractory chondrules, and in isolated refractory forsterites, can be formed by evaporation in which equilibrium was not always maintained. It is therefore possible that isolated refractory forsterites represent a more advanced evaporative stage of olivines, which originated in chondrules but were separated from their hosts, as suggested by Jones (1992) and Zanda et al. (2000).

4.4. Isotopic Data of Si

The δ^{29}Si and δ^{30}Si isotopic composition of the mesostasis in the charges of 1, 2, 4, 12 and 18 h runs are shown in Figure 6. The isotopic compositions are plotted against the molar Si/Al ratio in the mesostases of these charges normalized to the Si/Al ratio in the charge heated for only one hour. The 2 and 4-h runs show increasing Si/Al ratios due to the changing abundances of liquid and crystals during evaporation (Fig. 3), specifically evaporative loss of FeO, which causes the dissolution of olivine. Further loss of SiO_2 promotes crystallization of olivine, reversing the trend in Si/Al with heating time (Fig. 6). The Si-isotopic compositions of the melts exhibit increasing isotopic mass fractionation as heating times increase.

Several groups (e.g., Davis et al., 1990; Floss et al., 1996; Wang et al., 2001; Richter, 2003) have reported heavy isotope enrichments in Si, Mg and O in melt residues evaporated in vacuum and in H_2. The enrichments nearly follow the Rayleigh fractionation curves predicted for presumed evaporative species. The gas-liquid isotopic partition coefficients reported by these groups were systematically larger than theoretically expected (the inverse square root of the masses of the evaporating species). The reason for this is unclear. Floss et al. (1996) suggested that the deviation they observed was due to recondensation of the lighter isotope onto the surface of the charge in highly fractionated samples. Wang et al. (2001) rejected recon-

densation and proposed the involvement of heavier gas species during the evaporation process.

Linear regression lines through the data of the 12 and 18-h runs (dashed lines in Fig. 6) give higher alpha values as well. Theoretical isotopic partition coefficients for $^{29}Si/^{28}Si$ and for $^{30}Si/^{28}Si$ are 0.9888 and 0.9780, respectively, and the experimentally obtained alphas from this study were 0.9899 and 0.9805, respectively. The alpha values calculated from our experiments are not as large as those reported in other experimental studies (e.g., Floss et al. (1996) and Wang et al. (2001) report partition coefficients for $^{30}Si/^{28}Si$ of 0.9880 and 0.9860, respectively). One possible explanation is that Si/Al ratios in the 12 and 18-h runs decrease not only due to evaporation, but also due to olivine crystallization, leading to even lower calculated alpha values.

Measured $\delta^{29}Si$ and $\delta^{30}Si$ in individual chondrules or groups of chondrules from Allende (CV) and Dhajala (H3) from Clayton et al. (1985) all fall on a slope ½ line, similar to the results of our experiments (Fig. 6). In natural chondrules, however, $\delta^{29}Si$ values range between ~ -0.7 and 0.0‰ versus 0.57–13.88‰ in our experiments, and $\delta^{30}Si$ between ~ -1.5 and 0.0‰, versus 1.71–26.96‰ in our charges. The mean solar system value, based on the analysis of a large number of stony meteorites, is $\delta^{30}Si = -0.5$‰. Clayton et al. (1985) interpreted the isotopic enrichment observed in chondrules as the result of evaporation, but our study shows that even the slightest (several percent) evaporation of SiO_2 from a melt leads to a much larger fractionation (Fig. 6). However, if evaporation occurred in environments with high partial pressures of the species of interest where back reaction was effective, then evaporation loss is possible with less isotopic mass fractionation relative to a free evaporation regime (Alexander, 2004).

4.5. Back Reaction and the Suppression of Isotopic Mass Fractionation

The results reported above show that different degrees of evaporation of a CI-like material could produce the chemistry and mineralogy of chondrules, as well as their observed textures. However, isotope analyses of the evaporation residues exhibited strong enrichments in the heavy isotopes as in other evaporation experiments (e.g., Davis et al., 1990; Floss et al., 1996; Wang et al., 2001). Hence if chondrule melts had experienced free evaporation, systematic enrichments in heavy isotopes are expected in them as well.

Evaporation experiments on synthetic chondrule compositions resulted in rapid increases in $\delta^{41}K$ even at modest levels of evaporation (Yu et al., 2003). They showed that under conditions similar to those of transient heating events in the solar nebula (i.e., $P_{H2}=10^{-4}$ atm and 1723K), approximately 25% of Na and K was lost from a 50mg sample heated for ~1.5 min and immediately cooled at 5000K/h. Such a loss resulted in an isotopic mass fractionation of $\delta^{41}K \approx 7$‰ under Rayleigh conditions. Since chondrules were heated and melted at 1500–2100K, it is hard to imagine they could have possibly escaped evaporative loss (unless they were cooled at 10000–50,000K/h, which is much faster than the rates necessary to produce porphyritic and barred textures, i.e., 10–1000K/h).

Alexander et al. (2000) measured very large variations in $(K/Al)_L$, i.e., K/Al normalized to L-chondrite, in Bishunpur chondrules probably due to K loss, which would be expected if they were formed under nebula conditions, as is currently accepted. However, in general chondrules from Bishunpur and Semarkona lack significant K-isotopic fractionation (Alexander et al., 2000; Alexander and Grossman, 2000). Such observations have led to the conclusion that most of the chemical fractionation in the solar system occurred during the hot episode of the nebula when material condensed from gas to solids and that no significant volatile loss occurred in any of the processes following the condensation epoch, i.e., the chondrule-forming event (Humayun and Clayton, 1995). If volatile loss did in fact occur during chondrule formation, the lack of significant isotopic mass fractionation needs an explanation. Volatile loss during evaporation does not necessarily need to be accompanied by Rayleigh-isotopic mass fractionation. Esat (1996) stressed the importance of maintaining the highly restricted conditions required in Rayleigh distillation, i.e., the existence of a well-mixed reservoir and the complete removal of vaporized materials. If, for example, evaporation occurs rapidly with no time for maintaining a molten and well-mixed reservoir isotopic effects will be minimal.

An important way of achieving evaporative loss without significant isotopic fractionation is by back reaction between evaporating gases and the residual melt (Alexander et al., 2000; Nagahara and Ozawa, 2000a,b; Alexander and Wang, 2001; Alexander, 2004). Back reaction is essentially condensation from the ambient gas, due to increase in the abundance of gas species evaporating from a condensed phase. Nagahara and Ozawa (2000a,b) present a detailed theoretical demonstration of how back reaction affects isotopic mass fractionation. Alexander (2004) produced a model for chondrule evaporation in which mass fractionation was eliminated by gas-melt exchange.

In this study, we attempted to use the effect of back reaction at low pressure to suppress isotopic mass fractionation of K. Our results show that during evaporation, gases exchanging with the residual melts can effectively suppress the isotopic fractionation signature that would be associated with free evaporation. Although isotopic mass fractionation in the experimental charges was not completely eliminated to the degree observed in chondrules, the general expected effect was demonstrated.

In the chondrule-forming region, dust enrichment (i.e., higher initial dust to gas ratio) and the presence of the evaporating gases could have been important contributors to intensifying the effect of back reaction. The lack of significant isotopic mass fractionation in chondrules should therefore not be taken as proof for no evaporation. Open-system melting with back reaction is a feasible alternative to be considered.

4.6. Environments for Chondrule Formation

Models for the formation of chondrules generally fall into two main categories. In one, chondrule melts behaved as closed systems and in the second they experienced open-system melting, which included evaporation, recondensation and redox processes. In another scenario, chondrule formation occurred by direct condensation of solar nebula gas into liquids plus crystals (Blander and Katz, 1967; Ebel and Grossman, 1997, 2000; Georges et al., 2000; Weinbruch et al., 2000; Krot et al., 2001). It is impossible, from a geochemical perspective, to

differentiate between evaporative residues and direct condensates if they both achieved equilibrium with the ambient gas. However, the existence of relict grains in at least 15% of chondrules (Jones, 1996), believed to be fragments of a previous generation of chondrules, poses difficulties in explaining the origin of at least the "final" chondrule generation by condensation. In addition, attempts to match in detail the Na_2O contents of partially molten condensates with Types I and II chondrule compositions, using equilibrium thermodynamic calculations, have generally failed (Ebel and Grossman, 2000).

Flash heating of chondrule precursors was originally proposed as a mechanism by which the volatile elements present in many chondrules could survive evaporation in the canonical nebula. Also, some heating mechanisms proposed for the early stages of the solar nebula (e.g., lightning) were thought to require a rapid rise to peak temperature. However, experiments have shown that in the classical low-pressure, H_2-rich solar nebula, losses of volatiles are expected even with extremely short heating (Yu and Hewins, 1998; Yu et al., 2003). The present experiments suggest a heating time of several hours, which is compatible with the shock-heating model (Desch and Connolly, 2002). In addition, the presence of up to 3wt.% Na_2O in some chondrules coupled with the lack of evidence for free evaporation suggest that their heating did not occur in the canonical nebula (Alexander et al., 2000; Yu et al., 2003).

The constraints given by alkalis prompted the idea that chondrule formation might have occurred in a non-canonical nebular environment (e.g., Yu et al., 1996; Hewins et al., 1998; Alexander et al., 2000; Yu et al., 2003). Some proposed that their formation occurred in particle-rich opaque clouds with dust to gas enrichment of up to 500–1000× that of the canonical nebula (Wood, 1985; Wood and Hashimoto, 1993; Ebel and Grossman, 2000; Krot et al., 2001; Petaev et al., 2001; Lauretta et al., 2002). In such clouds, turbulence could have caused the concentration of chondrule-sized particles (Cuzzi et al., 1996). Chondrules could have exchanged with vapor produced by the evaporation of dust and the shocked gas would have kept them hot for several hours (Desch and Connolly, 2002).

This study attempted to show with two sets of experiments that chondrules could have experienced evaporation but not Rayleigh fractionation. Firstly, we explored the idea that chondrule precursors (i.e., CI material) were heated for substantial durations (1–18 h). We found that at $P_{H2}=1.3\times10^{-5}$ atm and T = 1580 °C, chondrule bulk and mineral compositions could be generated and, using experimentally obtained iron evaporation rates, calculated that Type IIA compositions required 0–0.65 h of heating, whereas Type IA compositions were produced after 3.1–3.7 h. These heating times were calculated assuming free evaporation under canonical nebula conditions. Naturally, if evaporation occurred in dust-rich environments heating times would be even longer. Secondly, we performed evaporation experiments in capsules, which retained part of the evolved K, and showed that K isotopic mass fractionation was much lower than that expected from Rayleigh fractionation.

Desch and Connolly (2002) show how cooling history is influenced by density of surviving unevaporated material. Following a transient-heating event (i.e., a shock wave) a heated domain cools by radiation from chondrules, with higher cooling rates for higher chondrule concentrations. We propose that the different chondrule types reflect formation in regions of different chondrule density. Type II chondrules formed in areas of high chondrule concentrations, where heating times were short and cooling rates high. In such regions evaporative loss would be minimal. Type I chondrules, on the other hand, formed in regions of lower chondrule concentrations, where long heating durations and slow cooling rates would allow substantial evaporative loss. In both cases, evaporation of dust concentrated in the clouds provided a suitable environment for back reaction between evaporated gas species and the residual melts. Back reaction is crucial for suppressing isotopic mass fractionation that is absent in chondrules.

5. CONCLUSIONS

A number of characteristics of chondrules, including bulk compositions, olivine compositions, chondrule size distribution and textures, can be produced by evaporation of a chondritic material under canonical nebula conditions. Open-system melting of a CI-like precursor can produce the bulk compositions of Type IIA and IA chondrules, by loss of FeO and SiO_2, with minimum formation times of 0–0.65 and 3.1–3.7 h, respectively. It can also produce the Ca-rich forsteritic olivine of Type IA and refractory chondrules. A starting material with a higher ratio of pyroxene to olivine is needed to produce Type IIB, IB and IAB compositions by evaporation.

Metallic iron, alkalis and sulfur were not present in any of the evaporative residues, which experienced free evaporation in low-pressure hydrogen. Similarly, these runs showed strong isotopic mass fractionation. However, charges run at the same pressures in capsules, where back reaction between evaporating gases and the residual melt was permitted, partially retained K and the isotopic mass fractionation of K was much less than the expected Rayleigh value.

Chondrules may have experienced open-system melting, but not free evaporation. To enable back reaction and recondensation, formation in dense clouds consisting of chondrules, dust with high partial pressure of lithophile elements is favored. Volatile-rich Type II chondrules may have formed in domains with high chondrule concentrations. Type I chondrules may come from domains with low chondrule concentrations and low cooling rates.

Acknowledgments—We are grateful to Yang Yu and Brigitte Zanda for helpful insights and discussion, Jeremy Delaney for help with electron probe analyses and imagery, the Muséum National d'Histoire Naturelle in Paris for starting materials and for the use of their electron probe, Jean Kozul for electro-plating apparatus, Mike Carr for analyzing samples on the DCP and Dr. S. A. Morse for providing Kiglapait olivine. We thank D. Ebel and C. Floss for detailed critical reviews, and D. Ebel for an annotated manuscript, which was invaluable in the revision process. This study was supported by NASA Cosmochemistry and Origins grants NAG5-4472, -4579 and -10494.

Associate editor: C. Koeberl

REFERENCES

Alexander C. M. O'D. (1994) Trace elements within ordinary chondrite chondrules: Implications for chondrule formation conditions and precursors. *Geochim. Cosmochim. Acta* **58,** 3451–3467.

Alexander C. M. O'D. (1996) Recycling and volatile loss in chondrule formation. In *Chondrules and the Protoplanetary Disk* (eds. R. H.

Hewins, R. H. Jones, and E. R. D. Scott), pp. 233–241. Cambridge Univ. Press, Cambridge.
Alexander C. M. O'D. (2004) Kinetic constraints for chondrule and CAI formation. *Geochim. Cosmochim. Acta* **68,** (in press).
Alexander C. M. O'D. and Grossman J. N. (2000) The K isotopes in Semarkona chondrules [abs.]. *Lunar Planet. Sci. XXXI*. Lunar Planet. Inst., Houston. CD-ROM #1850.
Alexander C. M. O'D. and Wang J. (2001) Iron isotopes in chondrules: Implications for the role of evaporation during chondrule formation. *Meteorit. Planet Sci.* **36,** 419–428.
Alexander C. M. O'D., Grossman J. N., Wang J., Zanda B., Bourot-Denise M., and Hewins R. H. (2000) The lack of potassium isotopic fractionation in Bishunpur chondrules. *Meteoritics and Planet Sci.* **35,** 859–868.
Anders E. and Grevesse N. (1989) Abundance of the elements: Meteoritic and solar. *Geochim. Cosmochim. Acta* **53,** 197–214.
Boss A. P. (1996) A concise guide to chondrule formation models. In *Chondrules and the Protoplanetary Disk* (eds. R. H. Hewins, R. H. Jones, and E. R. D. Scott), pp. 257–263. Cambridge Univ. Press, Cambridge.
Blander B. and Katz J. L. (1967) Condensation of primordial dust. *Geochim. Cosmochim. Acta* **31,** 1215–1238.
Brearley A. J. and Jones R. H. (1998) Chondritic meteorites. *Reviews in Mineralogy* **36,** 3-1–3-398.
Clayton R. N., Mayeda T. K., and Molini-Velsko C. A. (1985) Isotopic variations in solar system material: Evaporation and condensation of silicates. In *Protostars and Planets II* (eds. D. C. Black and M. S. Matthews), pp. 755–771. University of Arizona Press, Tucson, Arizona.
Cuzzi J. N., Dobrovolskis A. R., Hogan R. C. (1996) Turbulence, chondrules and planetesimals. In *Chondrules and the Protoplanetary Disk* (ed. R. H. Hewins, R. H. Jones, E. R. D. Scott), pp. 35-43, Cambridge University Press.
Davis A. M., Hashimoto A., Clayton R. N., and Mayeda T. K. (1990) Isotope mass fractionation during evaporation of Mg_2SiO_4. *Nature* **347,** 655–658.
Desch S. J. and Connolly H. C., Jr.. (2002) A model for the thermal processing of particles in solar nebula shocks: Application to cooling rates of chondrules. *Meteorit. Planet Sci.* **37,** 183–208.
Ebel D. S, Grossman L (1997) Direct condensation of ferromagnesian liquids from cosmic gases [abs.]. *Lunar Planet. Sci. XXVIII*. Lunar Planet. Inst., Houston. 317-318.
Ebel D. S. and Grossman L. (2000) Condensation in dust-enriched systems. *Geochim. Cosmochim. Acta* **64,** 339–366.
Ebel D. S., Engler A. and Kurat G. (2003) Pyroxene chondrules from olivine-depleted, dust-enriched systems [abs.]. *Lunar Planet. Sci. XXXIV*. Lunar Planet. Inst., Houston, CD-ROM #2059.
Esat T. M. (1996) Comment on "Potassium isotope cosmochemistry: Genetic implications of volatile element depletion." by Munir Humayun and R. N. Clayton. *Geochim. Cosmochim. Acta* **60,** 3755–3758.
Floss C., El Goresy A., Zinner E., Kransel G., Rammensee W., and Palme H. (1996) Elemental and isotopic fractionations produced through evaporation of the Allende CV chondrite: Implications for the origin of the HAL-type hibonite inclusions. *Geochim. Cosmochim. Acta* **60,** 1975–1997.
Georges P., Libourel G., and Deloule E. (2000) Experimental constraints on alkali condensation in chondrule formation. *Meteorit. Planet. Sci.* **35,** 1183–1188.
Govindaraju K. (1994) Compilation of working values and descriptions for 383 geostandards. *Geostandards Newsletter* **18,** 1–158.
Grossman J. N. (1988) Formation of chondrules. In *Meteorites and the Early Solar System* (eds. J. F. Kerridge and M. S. Matthews), pp. 680–696. University of Arizona, Arizona.
Grossman J. N. (1996) Chemical fractionations of chondrites: Signatures of events before chondrule formation. In *Chondrules and the Protoplanetary Disk* (eds. R. H. Hewins, R. H. Jones, and E. R. D. Scott), pp. 243–253. Cambridge Univ. Press, Cambridge.
Grossman J. N. and Wasson J. T. (1983a) The compositions of chondrules in unequilibrated chondrules: An evaluation of theories for the formation of chondrules and their precursor materials. In *Chondrules and their Origins* (ed. E. A. King), pp. 88-121, Lunar and Planetary Institute.
Grossman J. N. and Wasson J. T. (1983b) Refractory precursor components in Semarkona chondrules and the fractionation of refractory elements among chondrites. *Geochim. Cosmochim. Acta* **47,** 759–771.
Grossman J. N., Rubin A. E., Nagahara N., and King E. A. (1988) Properties of chondrules In *Meteorites and the Early Solar System* (eds. J. F. Kerridge and M. S. Matthews), pp. 680–696. University of Arizona, Arizona.
Hashimoto A. (1983) Evaporation metamorphism in the early solar nebular-evaporation experiments on the melt FeO-MgO-SiO_2-CaO-Al_2O_3 and chemical fractions of primitive material. *Geochem. J.* **17,** 111–145.
Herzberg C. T. (1979) The solubility of olivine in basaltic liquids: An ionic model. *Geochim. Cosmochim. Acta* **43,** 1241–1251.
Herzberg C. T. (1987) Magma density at high pressure Part 2: A test of olivine flotation hypothesis. In *Magmatic Processes: Physiochemical Principles* (ed. B. O. Mysen), 47–58, The Geochemical Society, Special Publication No. 1.
Hewins R. H. (1991) Retention of sodium during chondrule melting. *Geochim. Cosmochim. Acta* **55,** 935–942.
Hewins R. H., Yu Y., Zanda B., and Bourot-Denise M. (1997) Do nebular fractionation, evaporative losses, or both, influence chondrule compositions? *Antarct. Meteorite Res.* **10,** 275–298.
Hewins R. H., Zanda B., Yu Y. and Bourot-Denise M.(1998) Towards a new model for chondrules [abs.]. *Pellas Symposium, Muséum National d'Histoire Naturelle, Paris*. 31-34.
Huang S., Lu J., Prinz M., Weisberg M. K., Benoit P. H., and Sears D. W. G. (1996) Chondrules: Their diversity and the role of open-system processes during their formation. *Icarus* **122,** 316–346.
Humayun M. and Clayton R. N. (1995) Potassium isotope cosmochemistry: Genetic implications of volatile element depletion. *Geochim. Cosmochim. Acta* **59,** 2131–2148.
Jarosewich E. (1990) Chemical analyses of meteorites: A compilation of stony and iron meteorite analyses. *Meteoritics* **25,** 323–337.
Jones R. H. (1990) Petrology and mineralogy of Type II, FeO-rich chondrules in Semarkona (LL3.0): Origin by closed-system fractional crystallization, with evidence for supercooling. *Geochim. Cosmochim. Acta* **54,** 1785–1802.
Jones R. H. (1992) On the relationship between isolated and chondrule olivine grains in the carbonaceous chondrite ALHA77307. *Geochim. Cosmochim. Acta* **56,** 467–482.
Jones R. H. (1994) Petrology of FeO-poor, porphyritic pyroxene chondrules in the Semarkona chondrite. *Geochim. Cosmochim. Acta* **58,** 5325–5340.
Jones R. H. (1996) FeO-rich porphyritic pyroxene chondrules in unequilibrated ordinary chondrites. *Geochim. Cosmochim. Acta* **60,** 3115–3138.
Jones R. H, Scott E. R. D. (1989) Petrology and thermal history of type IA chondrules in Semarkona (LL3.0). *19th Proc. Lunar Planet. Sci. Conf.* Lunar Planet. Inst., Houston, 523-536.
Jurewicz A. J. G. and Watson E. B. (1988) Cations in olivine, Part 2: Diffusion in olivine xenocrysts, with applications to petrology and mineral physics. *Contrib. Mineral Petrol.* **99,** 186–201.
Köhler T. B. and Brey G. P. (1990) Calcium exchange between olivine and clinopyroxene calibrated as a geothermobarometer for natural peridotites from 2 to 60 kb with applications. *Geochim. Cosmochim. Acta* **54,** 2375–2388.
Krot A. N., Meibom A. M., Russell S. S., Alexander C. M. O'D., Jeffries T. E., and Keil K. (2001) A new astrophysical setting for chondrule formation. *Science* **291,** 1776–1779.
Kuroda D, Hashimoto A (2002) The reaction of forsterite with hydrogen–its apparent and real temperature dependences. *15thAntarct. Meteorite Res.*, National Institute of Polar Research, Tokyo, Japan. 152-164.
Lauretta D. S., Killgore M., Benoit P. H., Moore S., and Sears D. W. G. (2002) NWA505: A new LL3.0 chondrite with evidence for chondrule formation in a dust-rich environment [abs.]. *Meteorit. Planet Sci.* **37,** A84.
Libourel G. (1999) Systematics of calcium partitioning between olivine and silicate melt: Implications for melt structure and calcium content of magmatic olivines. *Contrib. Mineral Petrol.* **136,** 63–80.

Lofgren G. (1989) Dynamic crystallization of chondrule melts of porphyritic olivine composition: Textures experimental and natural. *Geochim. Cosmochim. Acta* **53,** 461–470.

Matsunami S., Ninagawa K., Nishimura S., Kubono N., Yamamoto I., Kohata M., Wada T., Yamashita Y., Lu J., Sears D. W. G., and Nishimura H. (1993) Thermoluminescence and compositional zoning in the mesostasis of a Semarkona group A1 chondrule and new insights into the chondrule-forming process. *Geochim. Cosmochim. Acta* **57,** 2101–2110.

McSween H. Y. (1977a) Chemical and petrographic constraints on the origin of chondrules and inclusions in carbonaceous chondrites. *Geochim. Cosmochim. Acta* **41,** 1843–1860.

McSween H. Y. (1977b) On the nature and origin of isolated olivine grains in carbonaceous chondrites. *Geochim. Cosmochim. Acta* **41,** 411–418.

Mullane E., Russell S. S., Gounelle M. and Mason T. F. D. (2003) Iron isotope composition of Allende and Chainpur chondrules: Effects of equilibration and thermal history [abs.]. *Lunar and Planet. Sci. XXXIV*. Lunar Planet. Inst., Houston, CD-ROM #1027.

Nagahara H. and Ozawa K. (1994) Vaporization rates of forsterite in hydrogen gas. *Meteoritics* **29,** 508–509.

Nagahara H. and Ozawa K. (1996) Evaporation of forsterite in H_2 gas. *Geochim. Cosmochim. Acta* **60,** 1445–1459.

Nagahara H. and Ozawa K. (2000a) Isotopic fractionation as a probe of heating processes in the solar nebula. *Chem. Geol.* **169,** 45–68.

Nagahara H, Ozawa K (2000b) The role of back reaction on chemical fractionation during evaporation of a condensed phase [abs.]. *Lunar Planet. Sci. XXXI*, Lunar Planet. Inst., Houston, CD-ROM #1340.

Petaev M. I., Meibom A., Krot A. N., Wood J. A., and Keil K. (2001) The condensation origin of zoned metal grains in Queen Alexandra Range 94411: Implications for the formation of the Bencubbin-like chondrites. *Meteorit. Planet Sci.* **36,** 93–106.

Richter F. M (2003) Time scales for elemental and isotopic fractionation by evaporation and condensation [abs.]. *Lunar Planet. Sci. XXXIV*. Lunar Planet. Inst., Houston, CD-ROM #1231.

Richter F. M., Davis A. M., Ebel D. S., and Hashimoto A. (2002) Elemental and isotopic fractionation of Type B calcium-, aluminium-rich inclusions: Experiments, theoretical considerations, and constraints on their thermal evolution. *Geochim. Cosmochim. Acta* **66,** 521–540.

Rubin A. E., Fegley B., and Brett R. (1988) Oxidation state of chondrites. In *Meteorites and the Early Solar System* (eds. J. F. Kerridge and M. S. Matthews), pp. 488–511. University of Arizona, Arizona.

Scott E. R. D. and Taylor G. J. (1983) Chondrules and other components in C, O and E chondrites: Similarities in their properties and origins. *14thProc. Lunar Planet. Sci. Conf.* Lunar Planet. Inst., Houston, B275-B286.

Scott E. R. D., Love S. G., and Krot A. N. (1996) Formation of chondrules and chondrites in the protoplanetary nebula. In *Chondrules and the Protoplanetary Disk* (eds. R. H. Hewins, R. H. Jones, and E. R. D. Scott), pp. 87–96. Cambridge Univ. Press, Cambridge.

Sears D. W. G., Huang S., and Benoit P. H. (1996) Open-system behavior during chondrule formation. In *Chondrules and the Protoplanetary Disk* (eds. R. H. Hewins, R. H. Jones, and E. R. D. Scott), pp. 221–231. Cambridge Univ. Press, Cambridge.

Steele I. M. (1986) Compositions and textures of relic forsterite in carbonaceous and unequilibrated ordinary chondrites. *Geochim. Cosmochim. Acta* **50,** 1379–1395.

Tissandier L., Libourel G., and Robert F. (2002) Gas-melt interactions and their bearing on chondrule formation. *Meteorit. Planet. Sci.* **37,** 1377–1389.

Tsuchiyama A., Nagahara H., and Kushiro I. (1981) Volatilization of sodium from silicate melt spheres and its application to the formation of chondrules. *Geochim. Cosmochim. Acta* **45,** 1357–1367.

Tsuchiyama A., Tachibana S., and Takahashi T. (1999) Evaporation of forsterite in the primordial solar nebula; rates and accompanied isotopic fractionation. *Geochim. Cosmochim. Acta* **63,** 2451–2466.

Wang J., Davis A. M., Clayton R. N., Mayeda T. K., and Hashimoto A. (2001) Chemical and isotopic fractionation during evaporation of the FeO-MgO-SiO_2-CaO-Al_2O_3-TiO_2 rare earth element melt system. *Geochim. Cosmochim. Acta* **65,** 479–494.

Weinbruch S., Palme H., and Spettel B. (2000) Refractory forsterite in primitive meteorites: Condensates from the solar nebula? *Meteorit. Planet. Sci.* **35,** 161–171.

Wood J. A. (1985) Meteoritic constraints on processes in the solar nebula: An overview. In *Protostars and Planets II* (eds. D. C. Black and M. S. Matthews), pp. 682–702. Univ. of Arizona Press, Tucson.

Wood J. A. and Hashimoto A. (1993) Mineral equilibrium in fractionated nebular systems. *Geochim. Cosmochim. Acta* **57,** 2377–2388.

Xiong Y, Hewins R. H (2003) Evaporation loss of light elements as a function of cooling rate: Logarithmic law [abs.]. *Lunar Planet. Sci. XXXIV*. Lunar Planet. Inst., Houston, CD-ROM #1206.

Yu Y. and Hewins R. H. (1998) Transient heating and chondrule formation: Evidence from sodium loss in flash heating simulation experiments. *Geochim. Cosmochim. Acta* **62,** 159–172.

Yu Y., Hewins R. H., and Zanda B. (1996) Sodium and sulfur in chondrules: Heating time and cooling curves. In *Chondrules and the Protoplanetary Disk* (eds. R. H. Hewins, R. H. Jones, and E. R. D. Scott), pp. 213–219. Cambridge Univ. Press, Cambridge.

Yu Y., Hewins R. H., Alexander C. M. O'D., and Wang J. (2003) Experimental study of evaporation and isotopic mass fractionation of potassium in silicate melts. *Geochim. Cosmochim. Acta* **67,** 773–786.

Zanda B., Libourel G., and Blanc P. (2000) Blue luminescing olivine-fassaite-spinel chondrules in the Allende meteorite [abs.]. *Meteorit. Planet Sci.* **35,** A176–A177.

Zhu X. K., Guo Y., O'Nions R. K., Galy A., Young E. D., and Ash R. D. (2001) Iron isotope cosmochemistry: High-precision isotope ratio measurement using MC-ICPMS [abs.]. *Meteoritics* **36,** A231.